Characteristics of Ring-Cusp Discharge Chambers

J. N. Matossian* and J. R. Beattie†
Hughes Research Laboratories, Malibu, California 90265

This paper describes comprehensive measurements of the operating characteristics of a 30-cm-diam ring-cusp ion thruster. The dominant mechanisms responsible for its high level of performance are discussed, and performance parameters are quantitatively compared with those representative of a 30-cm-diam, divergent-field J-series thruster. For the same discharge-chamber operating conditions, it is shown that the baseline beam-ion-production cost achieved by the ring-cusp thruster is 30 eV/ion lower than that of the J-series thruster. This high level of performance is correlated with measurements of the discharge-chamber plasma properties and with current-flow measurements to the anode- and cathode-potential surfaces of the discharge chamber. Compared to the J-series thruster design, the ring-cusp thruster design is shown to maintain both a higher primary-electron population and Maxwellian-electron temperature as the beam-ion-production cost is reduced to its baseline value. The role of the individual anode surfaces defining the discharge-chamber boundary is explored and it is shown that ion losses to the discharge-chamber walls can be reduced by an applied electrostatic field. A performance comparison of ring-cusp thruster operation on xenon and mercury propellants demonstrates that, for the same discharge-chamber operating conditions, operation with xenon propellant results in a significant reduction (≃ 15 eV/ion) in baseline beam-ion-production cost.

Nomenclature

B = magnetic field of strength, Wb/m^2
dl = infinitesimal path length, m
J_A = accelerator-electrode current, mA
J_{AS} = net current to anode surface, A
J_B = bias current of sidewall/endwall-plenum, A
J_b = extracted ion-beam current, A
J_E = cathode-emission current, A
J_{SG} = current collected by the screen grid, A
$\dot{m}$ = discharge-chamber propellant flow rate, equivalent A
$\bar{n}_m$ = volume-averaged Maxwellian-electron density, m^{-3}
$\bar{n}_p$ = volume-averaged primary-electron density, m^{-3}
R = net-to-total accelerating voltage, V_b/V_T
$\bar{T}_m$ = volume-averaged Maxwellian-electron temperature, eV
V_A = accelerator-electrode voltage, V
V_B = bias voltage of sidewall/endwall-plenum, V
V_b = beam voltage, V
V_D = discharge voltage, V
V_T = total voltage, $|V_A| + V_B$, V
β = correction factor for doubly charged ions
ϵ_i = beam-ion-production cost, $J_E V_D/J_b$, eV/ion
η_{md} = discharge propellant-utilization efficiency, $\beta J_b/\dot{m}$, % (corrected for doubly charged ions)
$(\eta_{md})_{unc}$ = discharge propellant-utilization efficiency, $J_b/\dot{m}$, % (uncorrected for doubly charged ions)

Presented as Paper IEPC-88-063 at the AIAA/DGLR 20th International Electric Propulsion Conference, Garmisch-Partenkirchen, Germany, Oct. 3-6, 1988; received Dec. 19, 1988; revision received April 7, 1990; accepted for publication April 24, 1990.

*Member of the Technical Staff, Plasma Physics Department. Member AIAA.

†Project Manager, Plasma Physics Department. Senior Member AIAA.

Introduction

RING-CUSP thruster technology[1,2] has had a significant effect on the design and performance of electron-bombardment ion thrusters. The inherent simplicity and demonstrated high level of performance characteristic of the ring-cusp thruster design offers significant advantages over the divergent-field J-series thruster design.[3,4] The high level of performance characteristic of the ring-cusp thruster is the result of the magnetic-field distribution used to confine the discharge-chamber plasma, as well as the distribution of anode- and cathode-potential surfaces defining the discharge-chamber boundary. The strong magnetic fields at the boundary of the discharge chamber inhibit energetic electrons from reaching the anode-potential surfaces anywhere except in the cusp regions of the magnetic field defined by the three magnet rings.[5] Energetic electrons are prevented from crossing the magnetic flux lines that connect adjacent magnet rings by the large values of $\int B dl$ (typically on the order of 10^{-3} Wb/m = 1000 G-cm).[2,6] Plasma electrons bound to magnetic field lines that intersect the anode are reflected from the magnet cusps due to mirror effects and limited conduction area.[2,7]

The magnetically shielded anode-potential surface of the discharge chamber limits the amount of ion loss. Both analytical[8] and experimental[9] investigations have shown that the ion-

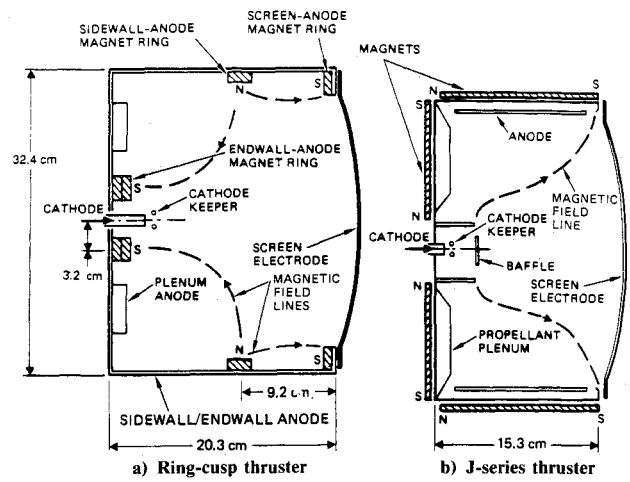

Fig. 1 Schematic diagram of the discharge chambers in ring-cusp and J-series thrusters.

arrival rate at these surfaces is consistent with the ions having a velocity close to that of the slow-moving neutrals. With nearly all of the discharge-chamber volume bounded by magnetically shielded anode-potential surfaces, ion loss in the ring-cusp discharge chamber is relatively low.

This paper describes the results of an investigation to support this description of the operating characteristics of the ring-cusp discharge chamber, including a comparison with the J-series thruster. The basic features distinguishing each thruster design are described, and the performance of each design is correlated with measurements of its discharge-chamber plasma properties. Current flow to the anode- and cathode-potential surfaces defining the ring-cusp discharge chamber is quantitatively correlated with thruster performance. By modifying the potential of each separate anode, the role of these surfaces on thruster performance is explored. A comparison of ring-cusp thruster operation on xenon and mercury propellants is presented to show that, for the same discharge-chamber operating conditions, thruster operation with xenon propellant results in a significant reduction ($\simeq$ 15 eV/ion) in baseline beam-ion-production cost.

Discharge-Chamber Design

Figure 1 shows a schematic diagram of a 30-cm-diam laboratory-model ring-cusp thruster. For comparison, a schematic diagram of a 30-cm-diam divergent-field J-series thruster[3,4] is also shown. The ring-cusp discharge-chamber design of Fig. 1 evolved as a result of a systematic investigation[5,10] aimed at simplifying the original Sovey design[1] while maintaining a high level of performance.

The ring-cusp discharge chamber is comprised of a cylindrical sidewall and circular endwall, both of which are made of soft iron and maintained at anode potential. The cathode and screen electrode are the only electrodes operated at cathode potential. The cathode and cathode keeper are positioned in the discharge chamber with no structure surrounding them.

The J-series discharge chamber, by contrast, is comprised of a circular endwall and a cylindrical outer shell that are operated at cathode potential, and a cylindrical inner liner that is operated at anode potential. The cathode is surrounded by a magnetic-baffle coil that can be energized to control the impedance between the cathode and main-discharge plasmas. The entire cathode assembly (consisting of the cathode and cathode keeper) is located within a baffle/pole-piece assembly that isolates the cathode and main-discharge plasmas.

The nature of the magnetic-field distribution for both thruster designs is suggested by dashed lines in Fig. 1. The cusp magnetic-field distribution within the ring-cusp discharge chamber is generated by three $SmCo_5$ permanent-magnet rings, two single-layer rings on the cylindrical sidewall, and one double-layer ring on the endwall. The magnets are held in place only by their magnetic attraction to the soft-iron boundary, which provides a low-reluctance path for closing the magnetic-flux lines.

By contrast, the divergent magnetic-field distribution within the J-series discharge chamber is generated by Alnico V permanent magnets arranged axially and radially along the outside of the chamber. The discharge-chamber boundary of the J-series thruster serves as a structural member and is not a part of the magnetic circuit.

Figure 2 compares the scalar magnetic-field distribution for the ring-cusp and J-series discharge chambers. The 0.0025-, 0.0050-, 0.0075-, and 0.01-Wb/m^2 (25-, 50-, 75-, and 100-G) contour lines are indicated. The most significant feature of the ring-cusp design is the existence of strong magnetic-field integrals (on the order of 10^{-3} Wb/m; 1000 G-cm) at the boundaries of its discharge chamber. By contrast, the J-series thruster exhibits a much weaker and nearly uniform scalar magnetic-field distribution.

Thruster Performance Measurements

The performance of an ion thruster is given by the variation of beam-ion-production cost with propellant-utilization efficiency. Figure 3 shows performance measurements (corrected for doubly charged ions) of the ring-cusp thruster operated on mercury propellant. Both the accuracy and precision of the performance measurements are greater than or equal to $\pm 2\%$. For each operating point along the performance curve, the beam current and discharge voltage are maintained constant within 1% of their values of 2 A and 32 V, respectively (the standard operating conditions for the majority of the results

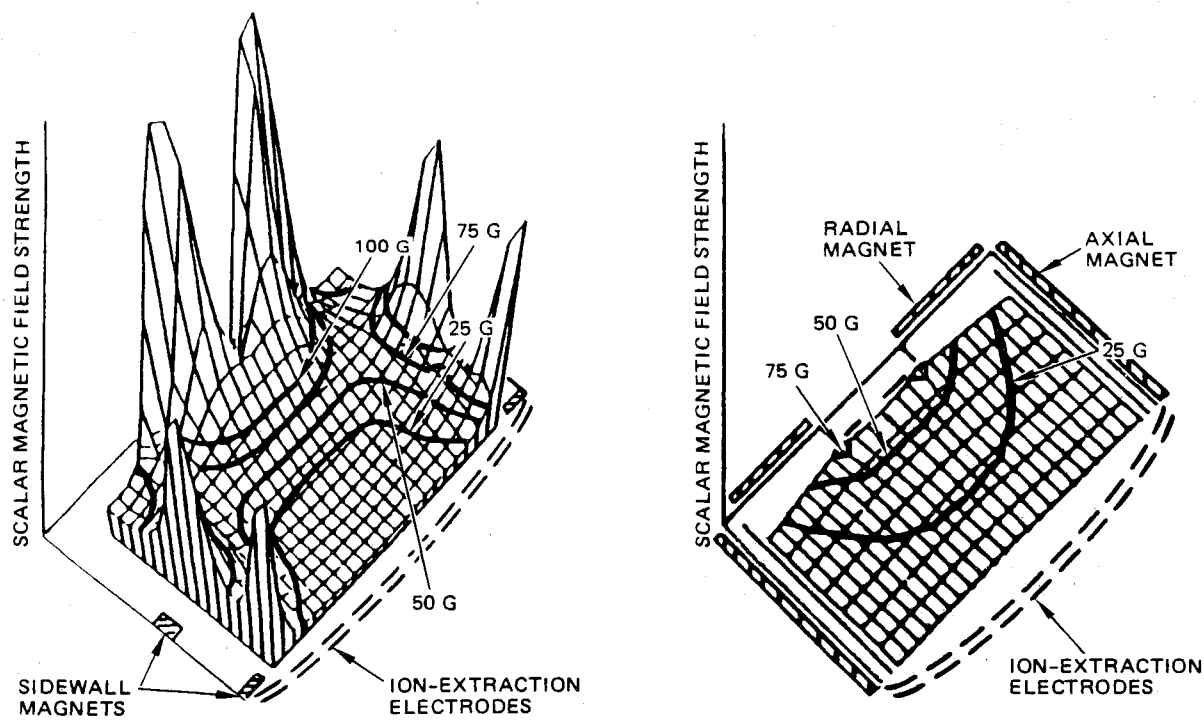

a) Ring-cusp thruster

b) J-series thruster

Fig. 2 Comparison of the scalar magnetic-field distributions in the ring-cusp and J-series thrusters.

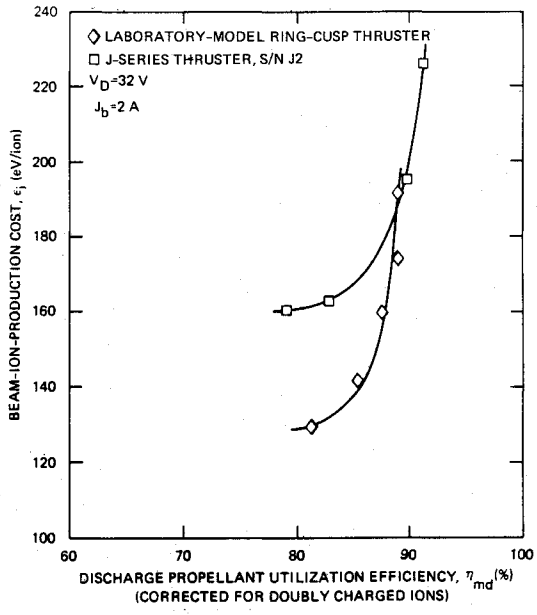

Fig. 3 Performance comparison of the ring-cusp and J-series thrusters (corrected for doubly-charged ions).

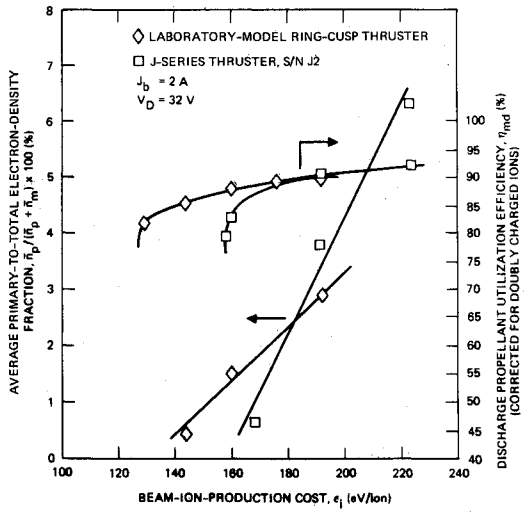

Fig. 4 Volume-averaged primary-electron fraction and discharge-chamber performance for the ring-cusp and J-series thrusters.

presented in this paper). For comparison, performance measurements for the J-series thruster (serial number S/N J2) operated at the same conditions as the ring-cusp thruster are also presented. Both thrusters used similar ion-optics assemblies in order to ensure that performance differences between the two thrusters were due solely to the discharge-chamber designs.

Figure 3 shows that the ring-cusp thruster can achieve a baseline beam-ion-production cost that is 30 eV/ion lower than it is for the J-series thruster. For a beam current of J_b = 2 A, this corresponds to a 60-W reduction in discharge power. The dominant factors responsible for this high level of performance include the magnetic-field distribution used to confine the discharge-chamber plasma and the distribution of anode- and cathode-potential surfaces defining the discharge-chamber boundary. In the sections to follow, we present experimental data (in the form of discharge-chamber plasma properties and current distribution) to support these results.

Plasma Properties

Plasma-property measurements provide a useful tool for explaining the performance differences between thrusters. In a previous publication,[11] we described a model for computing the volume-averaged plasma properties in electron-bombardment ion thrusters using spatially varying Langmuir-probe measurements. The model is based on a plasma-property averaging technique that transforms the spatially varying discharge-chamber plasma parameters into their equivalent, spatially uniform values. The model allows different thruster designs to be evaluated and compared on the basis of a single "average" value for each plasma parameter. Average values of the Maxwellian-electron temperature and density, as well as the primary-electron energy and density, were obtained and correlated with measured performance of the ring-cusp and J-series thrusters to explain the performance difference shown in Fig. 3.

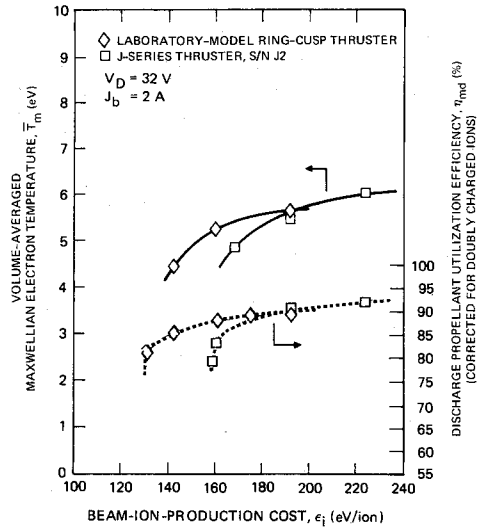

Fig. 5 Volume-averaged Maxwellian-electron temperature and discharge-chamber performance comparison for the ring-cusp and J-series thrusters.

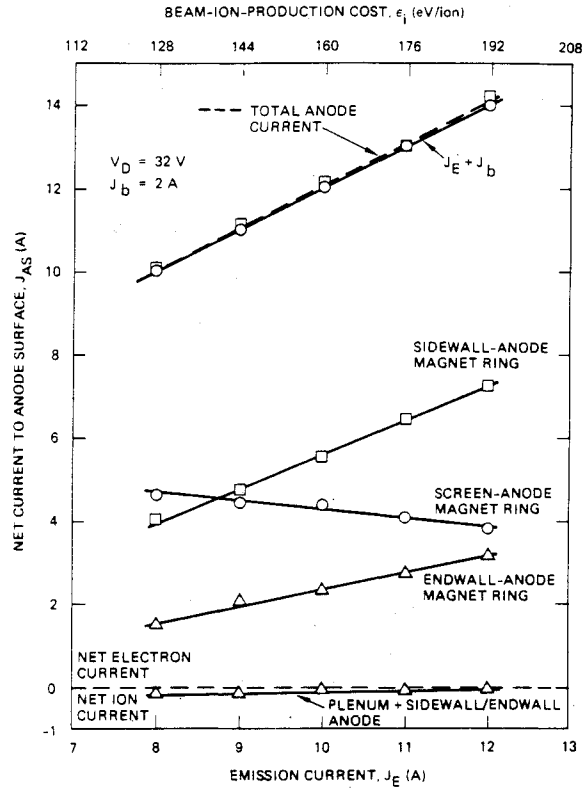

Fig. 6 Variation of net current collected by various anode surfaces with cathode-emission current.

Figure 4 shows the variation of the average primary-electron fraction (ratio of primary-electron density to plasma density) with beam-ion-production cost for both thrusters obtained using the volume-averaging technique.[11] For comparison, performance measurements for both thrusters are also shown (the performance data from Fig. 3 have been replotted in Fig. 4 with the propellant-utilization efficiency as the dependent variable).

The data presented in Fig. 4 are a comparison of the primary-electron fraction representative of each discharge-chamber design for the same primary-electron energy and beam current. The primary-electron energy is equal to the difference in energy between the cathode-keeper plasma potential and the discharge-chamber plasma potential. In a previous publication,[11] the primary-electron energy was measured for both thrusters and found to be nearly the same for operation at the same discharge voltage (32 V) and beam current (2 A).

For constant primary-electron energy, the primary-electron density is a function of only the propellant-utilization efficiency for a given thruster design.[11,12] Figure 4 demonstrates that for a constant propellant-utilization efficiency of 85%, for example, both thrusters achieve approximately the same primary-electron fraction. However, the ring-cusp thruster is able to operate at a beam-ion-production cost that is over 20 eV/ion lower than that of the J-series thruster. For a beam current of 2 A, this corresponds to a 40-W reduction in discharge power. (At the baseline beam-ion-production cost there is a 60-W reduction in discharge power compared to the J-series thruster.) Alternatively, for the same beam-ion-production cost of 160 eV/ion (the same discharge power) the ring-cusp thruster achieves a higher primary-electron fraction, consistent with its higher propellant-utilization efficiency. These results suggest that the ring-cusp discharge chamber is more efficient in confining primary electrons as the beam-ion-production cost is reduced to its baseline value. Although the primary-electron fraction is low, primary electrons are known to be responsible for up to 15% of the total ion production.[5,11]

The Maxwellian electrons are responsible for the balance of the ion production. The spatially varying Maxwellian-electron temperature for the ring-cusp and J-series thrusters was measured and found to be constant along the magnetic-field lines, with the isotherms having very nearly the same shape as the magnetic-field lines.[2,5,13] The volume-averaged Maxwellian-electron temperature was obtained from these measurements for each thruster design and the results are presented in Fig. 5.

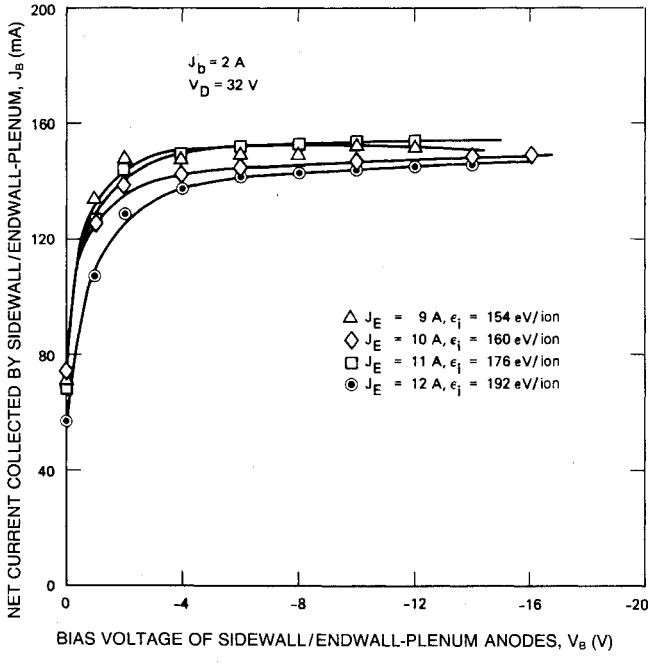

Fig. 7 Variation of net current collected by the sidewall/endwall-plenum with bias voltage.

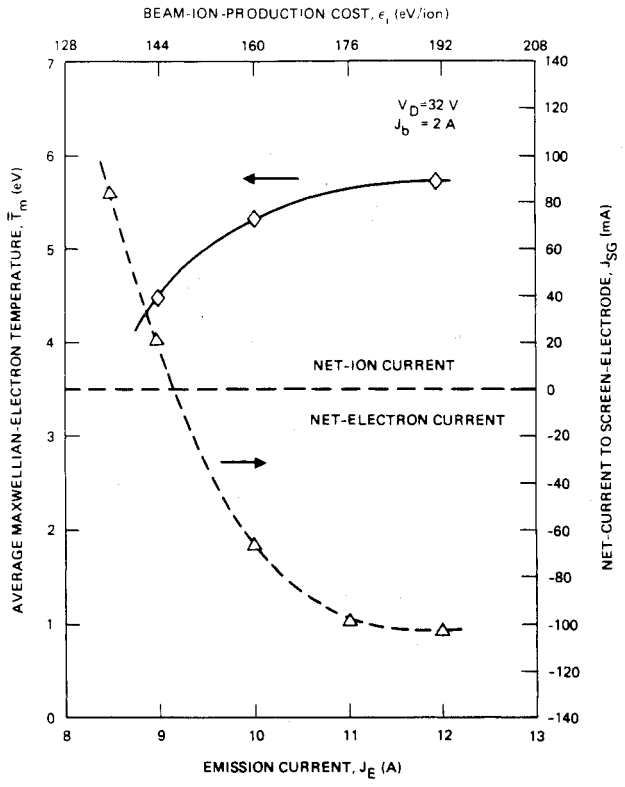

Fig. 8 Correlation of volume-averaged Maxwellian-electron temperature with net current collected by the screen electrode.

For constant primary-electron energy and beam current, the Maxwellian-electron temperature is a function of only the propellant-utilization efficiency for a given thruster design.[11,12] Figure 5 demonstrates that at a propellant-utilization efficiency of 85%, for example, the two thrusters achieve the same electron temperature. However, the ring-cusp thruster is able to operate at a beam-ion-production cost that is over 20 eV/ion lower (a 40-W reduction in discharge power) than that of the J-series thruster. Alternatively, for the same beam-ion-production cost (ϵ_i = 160 eV/ion), the ring-cusp thruster achieves a higher Maxwellian-electron temperature than the J-series thruster does, which is consistent with its higher propellant-utilization efficiency. These results suggest that the ring-cusp thruster is more efficient than the J-series thruster in confining Maxwellian electrons.

Discharge-Chamber Current Distribution

The plasma-property measurements presented in Figs. 4 and 5 help to understand the performance improvement of the ring-cusp thruster compared to the J-series thruster. For the same discharge-chamber operating conditions, primary and Maxwellian electrons are more efficiently confined by the ring-cusp design, resulting in a lower beam-ion-production cost (discharge power) to achieve a given propellant-utilization efficiency.

To provide additional understanding of the operating characteristics of the ring-cusp discharge-chamber, we measured the ion and electron currents to the anode- and cathode-potential surfaces of the discharge chamber and then correlated them with thruster performance measurements. For the ring-cusp discharge chamber, there is excellent electron confinement to the three anode-potential magnet rings. Net ion current is collected by the magnetically shielded anode-potential boundary of the discharge chamber. As the beam-ion-production cost is reduced to its baseline value, the current collected by the cathode-potential screen electrode makes a transition from net-electron to net-ion current, which correlates well with the behavior of the Maxwellian-electron temperature with thruster performance. In the sections below, we

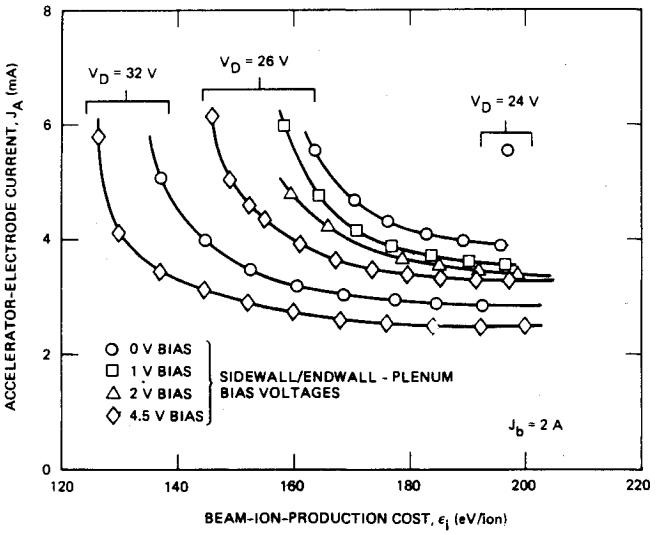

Fig. 9 Variation of accelerator-electrode current with beam-ion-production cost for different discharge voltages and sidewall/endwall-plenum bias voltages.

provide further description of these results. Details of the measurement techniques used can be found elsewhere.[5]

Anode-Potential Electrodes

Figure 6 shows the variation of the net currents collected by the five anode-potential surfaces as a function of cathode-emission current. For constant discharge voltage and beam current, the cathode-emission current determines the value of the beam-ion-production cost (see Nomenclature). The variation of total anode current (the sum of the individual anode currents) is also presented, showing that all net currents are satisfactorily accounted for.

The plenum and sidewall/endwall each collect a small net-ion current, on the order of 10 mA for the plenum and 60 mA for the sidewall/endwall. For clarity, the sum of these two currents is shown. By contrast, the screen-, sidewall-, and endwall-anode magnet rings collect net-electron current. These results suggest excellent electron confinement to the three magnet rings that define the cusp regions of the magnetic field.

The ion current collected by the sidewall/endwall and plenum surfaces was measured by simultaneously biasing these surfaces negative with respect to the remaining anode-potential surfaces. Figure 7 shows the variation of the net current collected by these surfaces with bias voltage for several thruster operating points. The ion current collected by the sidewall/endwall-plenum surface is about 145 mA ($\simeq$ 7% of the 2-A beam current). The electron current collected by the sidewall/endwall-plenum surface, obtained by subtracting the net-ion current collected at zero bias, is about 75 mA. The ion current saturates at a relatively low value of applied bias voltage ($\simeq$ 2 V), confirming that the electrons flowing to the sidewall/endwall-plenum surface have low energy.

The sidewall/endwall-plenum satisfies the definition of a magnetically shielded anode-potential surface. The small current of low-energy electrons collected by this surface confirms the confinement of high-energy electrons to the cusp regions of the magnetic field. The small ion current collected by this surface is consistent with the concept of reduced ion transport to a magnetically shielded anode-potential surface.[8,9] Both analytical[8] and experimental[9] investigations have shown that the ion-arrival rate at these surfaces is consistent with the ions having a velocity close to that of the slow-moving neutrals. With nearly all of the discharge-chamber volume bounded by magnetically shielded anode-potential surfaces, ion loss in the ring-cusp discharge chamber is relatively low.

Although we did not measure the ion loss to the three magnet rings, the concept of reduced ion transport to magnetically shielded anode-potential surfaces can be used to infer a small ion loss to the cusps as well. Kaufman[8] argues that the use of a strong, cusped magnetic field creates a density gradient of electrons which directs ion flow away from cusp regions, as well as from magnetically shielded anode-potential regions. Performance modeling of the ring-cusp thruster using the experimental data presented in this paper and the thruster performance model of Brophy[12] predicts that the calculated ion loss to all of the anode-potential surfaces of the ring-cusp discharge chamber is about 5%[14] of the total extracted ion-beam current of J_b = 2 A. The small ion current collected by the sidewall/endwall-plenum surface ($\simeq$ 7% of the 2-A beam current) is consistent with this result.

Cathode-Potential Electrodes

The cathode and screen electrode are the only cathode-potential surfaces within the ring-cusp discharge chamber. The screen electrode is a loss surface for ions, as well as energetic electrons capable of overcoming the potential difference between it and the plasma. The ion current collected by the screen electrode was determined by biasing it negative with respect to the cathode. The saturated ion current measured in this manner was 500 mA when the beam current was 2 A, implying an ion transmission of 80% for the particular ion-extraction assembly used in the test (serial number S/N 914).

Measurements of the variation of the net screen-electrode current with cathode-emission current (beam-ion-production cost) were obtained with the screen electrode connected to the cathode through an ammeter. Figure 8 shows that, as the cathode-emission current is reduced, the screen electrode undergoes a transition from net-electron to net-ion current collection. For comparison, calculations of the volume-averaged Maxwellian-electron temperature shown previously in Fig. 5 are also included in Fig. 8.

The transition from net-ion to net-electron current can be understood from the behavior of the Maxwellian-electron temperature. As the cathode-emission current is increased, the Maxwellian-electron temperature becomes high enough for electron collection by the cathode-potential screen electrode to

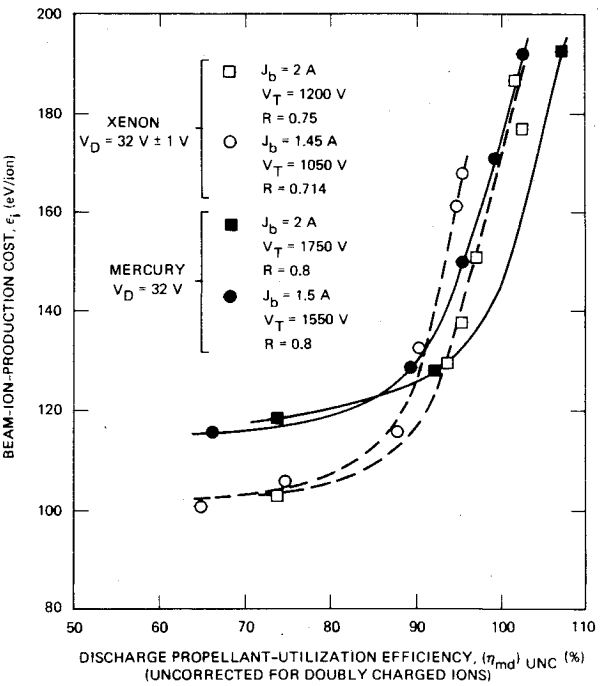

Fig. 10 Thruster performance measurements (uncorrected for doubly charged ions) for the ring-cusp thruster operated with mercury and xenon propellants at two beam-current levels.

be energetically possible. For a 32-V discharge, this requires an electron temperature in excess of about 4 eV.[5] Measurements of the spatially varying Maxwellian-electron temperature upstream of the screen electrode show good correlation with this result,[5] as do the volume-averaged electron temperature measurements included in Fig. 8.

Role of Anodes on Thruster Performance

Measurements of the discharge-chamber current distribution in the ring-cusp thruster indicate that electron current flow is primarily confined to the three anode-potential magnet rings. The magnetically shielded anode-potential discharge-chamber boundary collects a small net-ion current. We sought to explore the role of each of these anode-potential surfaces on thruster performance in order to gain additional physical insight into the operating characteristics of the ring-cusp discharge chamber. This was accomplished by allowing each separate anode surface to electrically float by disconnecting it from the discharge power supply, and then measuring the effect on thruster performance. The results of this investigation indicate that the sidewall- and screen-anode magnet rings are the dominant anode surfaces affecting thruster performance. The endwall-anode magnet ring was found to have little effect on thruster performance. The magnetically shielded discharge-chamber boundary (sidewall/endwall-plenum) significantly affects ion loss within the discharge chamber. Electrically floating this anode surface reduced the baseline beam-ion-production cost by 6 eV/ion.[5] This is believed to be due to a reduction in ion loss to its surface. The sidewall/endwall-plenum normally collects net-ion current (cf. Fig. 6). However, when this surface is allowed to float, its floating potential is positive relative to anode potential, which should retard ion flow to its surface.

We explored whether this result could be exploited to achieve an improvement in thruster performance by biasing the discharge-chamber boundary (sidewall/endwall-plenum) positive with respect to the three magnet rings. This is a technique known as "electrostatic ion plugging," which has been used by several researchers[15–17] to improve the performance of electron-bombardment-type ion sources.

Figure 9 shows the variation of accelerator-electrode current with beam-ion-production cost for different discharge voltages and sidewall/endwall-plenum bias voltages. The variation of accelerator-electrode current with beam-ion-production cost can be used as a fast technique to infer thruster performance. The reason for this is that the accelerator-electrode current primarily results from charge-exchange ion current produced in the inter-electrode and downstream regions of the ion-extraction assembly, and this current is directly proportional to the neutral loss rate from the discharge chamber. As the propellant-utilization efficiency is reduced with the beam current held fixed, the neutral loss rate increases, resulting in an increase in accelerator-electrode current. The variation of accelerator-electrode current with beam-ion-production cost can therefore be used as a relative indication of maximum propellant-utilization efficiency and as an absolute indication of baseline beam-ion-production cost.

The beam-ion-production cost was computed from the following relation:

$$\epsilon_i = \frac{J_E V_D}{J_b} + \frac{J_B V_B}{J_b} \qquad (1)$$

The results of Fig. 9 demonstrate that for thruster operation at the nominal discharge voltage of $V_D = 32$ V, the baseline beam-ion-production cost can be reduced by 10 eV/ion (a 20-W reduction in discharge power) for a 4.5-V bias voltage. With this bias voltage, the baseline beam-ion-production cost is reduced by 20 eV/ion (40-W reduction in discharge power) for thruster operation at a discharge voltage of $V_D = 26$ V.

Discharge-Chamber Performance with Different Propellants

The performances of the ring-cusp and J-series thrusters have been compared for similar discharge-chamber operating conditions. For the same propellant, the performance measurements presented in Fig. 3 showed that the ring-cusp thruster can achieve a baseline beam-ion-production cost that is 30 eV/ion lower than that of the J-series thruster. To understand the effect of propellant type on the baseline beam-ion-production cost, we compared the performance of the ring-cusp thruster operated on mercury and xenon propellants. Measurements were conducted using a 30-cm-diam ring-cusp thruster that allowed operation with either mercury or xenon propellant. Discharge-chamber performance comparisons were conducted at the same discharge voltage (same primary-electron energy) and beam current to ensure that performance differences were due to propellant type only.

Figure 10 shows a comparison of measured performance (uncorrected for doubly charged ions) for thruster operation at two different beam-current levels with xenon and mercury propellants. The performance measurements were obtained with an ion-extraction assembly that employed a 0.254-mm-thick (10-mil) screen electrode, whereas the performance measurements presented in the previous sections of this paper were obtained using a 0.381-mm-thick (15-mil) screen electrode. For thruster operation at 2 A of beam current, a significant reduction in baseline beam-ion-production cost was achieved using the grid set with the 0.254-mm-thick screen electrode. This performance improvement can be seen by comparing the baseline beam-ion-production cost for the ring-cusp thruster shown in Figs. 3 and 10. For a beam current of 2 A, Fig. 10 demonstrates that there is a reduction of about 12 eV/ion in the baseline beam-ion-production cost using the 0.254-mm-thick screen electrode. This behavior was previously documented[5,10] and is due to increased deflection of ions into the apertures of the screen electrode.[18]

For thruster operation at the baseline beam-ion-production cost, the doubly charged ion fraction is known to be negligible due to the low propellant-utilization efficiency.[5,6,10,12] Under these conditions, a valid performance comparison of the effect of propellant type can be made using the results shown in Fig. 10. As the figure shows, the baseline beam-ion-production cost is dependent on propellant type, but relatively independent of the beam current. Thruster operation on xenon propellant results in a reduction of about 15 eV/ion in the baseline beam-ion-production cost compared to operation on mercury.

The reduced baseline beam-ion-production cost can be explained using the thruster-performance model of Brophy,[12] on the basis of either a higher extracted beam-ion fraction, or a reduced baseline plasma-ion-production cost for xenon compared to mercury. The physical basis for the latter interpretation lies in the fact that while it takes less energy to ionize mercury compared to xenon, mercury has a lower threshold for excitation, which contributes to a lower threshold for energy losses. Theoretical modeling[14] to support this interpretation has been verified using the experimental results presented in this paper and the performance model of Brophy.[12]

Conclusions

The operating characteristics of the 30-cm-diam ring-cusp thruster have been described, including a comparison with the J-series thruster. The high level of performance characteristic of the ring-cusp thruster is the result of the magnetic-field distribution used to confine the discharge-chamber plasma as well as the anode- and cathode-potential surface distribution defining the discharge chamber. The ring-cusp discharge chamber confines plasma electrons more efficiently than the J-series thruster. For the same beam-ion-production cost, the average Maxwellian-electron temperature and primary-electron energy in the ring-cusp thruster is higher than it is in the J-series thruster. Ion loss in the ring-cusp discharge cham-

ber is low, consistent with its magnetically shielded anode-potential boundary.

The role of each separate anode surface defining the ring-cusp discharge chamber was explored. The magnetically shielded boundary significantly affects ion loss within the discharge chamber. By modifying the potential of this surface, enhanced thruster performance at reduced discharge voltage was realized. A performance comparison of ring-cusp thruster operation on xenon and mercury propellants was conducted. Thruster operation with xenon propellant results in a reduction of about 15 eV/ion in the baseline beam-ion-production cost compared to operation with mercury. This can be accounted for by a lower threshold for excitation with mercury which contributes to higher energy losses in the discharge chamber.

Acknowledgments

The authors wish to express their gratitude to Paul J. Wilbur of Colorado State University for valuable technical discussions and for performing the performance calculations for xenon and mercury propellants. We also acknowledge R. L. Maheux for providing technical assistance with the thruster-performance measurements. Work was performed in part under NASA Contract NAS 3-23775 and in part under a Hughes IR&D project.

References

[1]Sovey, J. S., "Improved Ion-Containment Using a Ring-Cusp Ion Thruster," AIAA Paper 82-1928, Nov. 1982.

[2]Beattie, J. R., and Poeschel, R. L., "Ring-Cusp Ion Thrusters," IEPC Paper 84-71, May, 1984.

[3]Lovell, R. R., et al., "30-cm Ion Thruster Subsystem Design Manual," NASA TM 79191, June 1979.

[4]Poeschel, R. L., "Retrofit and Acceptance Test of 30-cm Ion Thrusters," NASA CR-165259, Hughes Research Labs., Malibu, CA, June 1981.

[5]Beattie, J. R., and Matossian, J. N., "Mercury Ion Thruster Technology," NASA CR-174974, Hughes Research Labs., Malibu, CA, March 1989.

[6]Beattie, J. R., "Extended Performance Technology Study; 30-cm Thruster," NASA CR-168259, Hughes Research Labs., Malibu, CA, June 1983.

[7]Leung, K. N., Hershkowitz, N., and Mackenzie, K. R., "Plasma Confinement by Localized Cusps," *Physics of Fluids,* Vol. 19, No. 7, 1976, pp. 1045–1053.

[8]Kaufman, H. R., Robinson, R. S., and Frisa, L. E., "Ion Flow Experiments in a Multipole Discharge Chamber," *AIAA Journal,* Vol. 22, No. 11, 1984, pp. 1544–1549.

[9]Brophy, J. R., and Wilbur, P. J., "The Flexible Magnetic Field Thruster," *Journal of Spacecraft and Rockets,* Vol. 22, No. 6, 1983, pp. 611–618.

[10]Beattie, J. R., and Matossian, J. N., "Inert Gas Thruster Technology," Final Rept. NAS 3-23860, Hughes Research Labs., Malibu, CA, 1989.

[11]Matossian, J. N., and Beattie, J. R., "Model for Computing Volume-Averaged Plasma Properties in Electron-Bombardment Ion Thrusters," *Journal of Propulsion and Power,* Vol. 5, No. 2, 1989, pp. 188–196.

[12]Brophy, J. R., "Ion Thruster Performance Model," NASA CR-174810, Colorado State Univ., Fort Collins, CO, Dec. 1984.

[13]Longhurst, G., "Prediction of Plasma Properties in Mercury Ion Thrusters," NASA CR-159448, Colorado State Univ., Fort Collins, CO, Dec. 1978.

[14]Wilbur, P. J., "Advanced Electric Propulsion and Space Plasma Contactor Research," NASA CR-175119, Colorado State Univ., Fort Collins, CO, Jan. 1986.

[15]Goebel, D. M., "Ion Source Discharge Performance and Stability," *Physics of Fluids,* Vol. 25, No. 6, 1982, pp. 1093–1102.

[16]Ehlers, K. W., and Leung, K. N., "Increasing the Efficiency of a Multicusp Ion-Source," *Review of Scientific Instruments,* Vol. 53, No. 9, 1982, pp. 1429–1433.

[17]Hershkowitz, N., Hendricks, K., and Carpenter, R. T., "Electrostatic Plugging of Leaks in a Multipole Device," *Journal of Applied Physics,* Vol. 53, No. 6, 1982, pp. 4105–4112.

[18]Aston, G., "The Screen Hole Plasma Sheath of an Ion Accelerator System," AIAA Paper 79-2114, Oct. 1979.